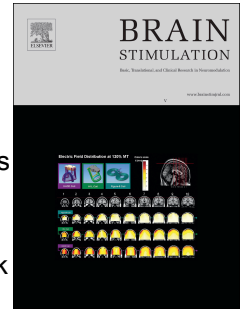


Journal Pre-proof



Ultrasound modulates neuronal potassium currents via ionotropic glutamate receptors

Benjamin Clennell, Tom G.J. Steward, Kaliya Hanman, Tom Needham, Janette Benachour, Mark Jepson, Meg Elley, Nathan Halford, Kate Heesom, Eunju Shin, Elek Molnár, Bruce W. Drinkwater, Daniel J. Whitcomb

PII: S1935-861X(23)01676-5

DOI: <https://doi.org/10.1016/j.brs.2023.01.1674>

Reference: BRS 2318

To appear in: *Brain Stimulation*

Received Date: 19 October 2022

Revised Date: 27 January 2023

Accepted Date: 27 January 2023

Please cite this article as: Clennell B, Steward TGJ, Hanman K, Needham T, Benachour J, Jepson M, Elley M, Halford N, Heesom K, Shin E, Molnár E, Drinkwater BW, Whitcomb DJ, Ultrasound modulates neuronal potassium currents via ionotropic glutamate receptors, *Brain Stimulation* (2023), doi: <https://doi.org/10.1016/j.brs.2023.01.1674>.

This is a PDF file of an article that has undergone enhancements after acceptance, such as the addition of a cover page and metadata, and formatting for readability, but it is not yet the definitive version of record. This version will undergo additional copyediting, typesetting and review before it is published in its final form, but we are providing this version to give early visibility of the article. Please note that, during the production process, errors may be discovered which could affect the content, and all legal disclaimers that apply to the journal pertain.

© 2023 Published by Elsevier Inc.

CRediT Author Statement

Benjamin Clennell: Conceptualization; Data curation; Formal analysis; Investigation; Methodology; Visualization; Roles/Writing -original draft; Writing -review & editing.

Tom G.J. Steward: Conceptualization; Formal analysis; Investigation; Methodology; Roles/Writing -original draft; Writing -review & editing.

Kaliya Hanman: Investigation; Methodology.

Tom Needham: Investigation; Methodology.

Janette Benachour: Investigation; Methodology; Visualization

Mark Jepson: Investigation; Resources; Methodology.

Meg Elley: Investigation; Methodology.

Nathan Halford: Investigation; Methodology.

Kate Heesom: Data curation; Formal analysis; Investigation; Resources; Methodology.

Eunju Shin: Conceptualization; Funding acquisition; Supervision.

Elek Molnár: Conceptualization; Methodology; Supervision; Writing -review & editing.

Bruce W. Drinkwater: Conceptualization; Funding acquisition; Methodology; Supervision; Writing -review & editing.

Daniel J. Whitcomb: Conceptualization; Data curation; Funding acquisition; Methodology; Project administration; Resources; Supervision; Roles/Writing -original draft; Writing -review & editing.

Ultrasound modulates neuronal potassium currents via ionotropic glutamate receptors

Benjamin Clennell^a, Tom G.J. Steward^a, Kaliya Hanman^b, Tom Needham^b, Janette Benachour^b, Mark Jepson^c, Meg Elley^a, Nathan Halford^a, Kate Heesom^d, Eunju Shin^e, Elek Molnár^b, Bruce W. Drinkwater^f & Daniel J. Whitcomb^{a*}

^aBristol Medical School, Faculty of Health Sciences, University of Bristol, Bristol, BS1 3NY, UK

^bSchool of Physiology, Pharmacology and Neuroscience, University of Bristol, Bristol, BS8 1TD, UK

^cWolfson Bioimaging Facility, Faculty of Life Sciences, University of Bristol, Bristol, BS8 1TD, UK

^dProteomics Facility Faculty of Life Sciences, University Walk, University of Bristol, Bristol, BS8 1TD, UK

^eSchool of Life Sciences, Keele University, ST5 5BG

^fFaculty of Engineering, University of Bristol, Bristol, BS8 1TR, UK

*Corresponding author: D.J.Whitcomb@Bristol.ac.uk

Abstract

Background: Focused ultrasound stimulation (FUS) has the potential to provide non-invasive neuromodulation of deep brain regions with unparalleled spatial precision. However, the cellular and molecular consequences of ultrasound stimulation on neurons remains poorly understood. We previously reported that ultrasound stimulation induces increases in neuronal excitability that persist for hours following stimulation *in vitro*. In the present study we sought to further elucidate the molecular mechanisms by which ultrasound regulates neuronal excitability and synaptic function.

Objectives: To determine the effect of ultrasound stimulation on voltage-gated ion channel function and synaptic plasticity.

Methods: Primary rat cortical neurons were exposed to a 40 s, 200 kHz pulsed ultrasound stimulus or sham-stimulus. Whole-cell patch clamp electrophysiology, quantitative proteomics and high-resolution confocal microscopy were employed to determine the effects of ultrasound stimulation on molecular regulators of neuronal excitability and synaptic function.

Results: We find that ultrasound exposure elicits sustained but reversible increases in whole-cell potassium currents. In addition, we find that ultrasound exposure activates synaptic signalling cascades that result in marked increases in excitatory synaptic transmission. Finally, we demonstrate the requirement of ionotropic glutamate receptor (AMPA/NMDAR) activation for ultrasound-induced modulation of neuronal potassium currents.

Conclusion: These results suggest specific patterns of pulsed ultrasound can induce contemporaneous enhancement of both neuronal excitability and synaptic function, with implications for the application of FUS in experimental and therapeutic settings. Further study is now required to deduce the precise molecular mechanisms through which these changes occur.

Introduction

Ultrasound is typically associated with medical diagnostic imaging, where pulse echo in the 1-10MHz range is used to visualise anatomical structures and does not induce detectable biological responses or adverse effects. In contrast, when ultrasound is delivered at lower frequencies, in the 0.2-1MHz range, brain activity can be modified^{1,2} and cognitive effects induced³⁻⁵. In this regard, focused ultrasound stimulation (FUS) is increasingly being recognised as an effective and precise non-invasive neuromodulator, alongside the more established approaches of transcranial direct current stimulation (tDCS)⁶ and transcranial magnetic stimulation (TMS)⁷. Indeed, a wealth of studies now describe the application of FUS in the modulation of neural function in humans⁸⁻²⁰ and non-human animals^{3,21-23}, with significant advantages over TMS and tDCS in terms of spatial focality and penetration depth. These neuromodulatory effects have been exploited experimentally, for example to delineate the contribution of the primate medial frontal cortex in decision-making²⁴. In addition, recent evidence points towards the possibility of using FUS for therapeutic purposes, with potential interventions in Alzheimer's¹⁶ and Parkinson's disease²⁵, pain conditions⁵ and mood disorders¹⁰.

Despite the numerous reports of the functional consequences and potential applications of FUS, we still do not understand the cellular and molecular mediators of the described effects. Mechanistic studies are largely confined to the immediate cellular response to FUS. Here various effects are reported, including induction of action potential firing^{26,27}, modulation of voltage-gated ion-channel currents²⁷, calcium responses²⁸, and stimulation of synaptic transmission²⁹. These are variously attributed to mechanosensitive channels³⁰, pore-formation³¹, membrane cavitation³² and glial cell activation³³ as key cellular transducers of ultrasound. However, FUS has been demonstrated to induce target specific, bidirectional changes to functional connectivity, as well as changes to cortical excitability, that persist up to 2-hours *in vivo*³⁴⁻³⁶, suggesting that FUS induces lasting functional change to neurons and

synapses. The mechanisms by which these persistent, FUS-induced changes to neural circuits manifest, however, remains poorly understood.

We previously reported that brief ultrasound exposure, delivered over 40s, increased neuronal excitability in primary cultured cortical rat neurons, with effects lasting for several hours³⁷. Our data indicated that the changes to excitability occurred in conjunction with modified action potential kinetics. Consistent with this, previous studies have shown that ultrasound can reversibly modulate $Na_v1.5$, TREK-1, TREK-2, and TRAAK ion channel currents when expressed in *Xenopus oocytes*³⁸. In addition, ultrasound was shown to evoke action potentials in hippocampal slices and induce SNARE-mediated synaptic vesicle exocytosis³⁹. Similarly, ultrasound was shown to elicit action potentials and increase firing frequency in hippocampal CA1 pyramidal neurons^{40,41}. These studies also reported changes to action potential waveforms, and input resistance, as well as modulation of voltage-gated sodium⁴⁰ and potassium currents⁴¹. Together, these findings support the notion that TUS regulates the molecular determinants of action potential function; however, they provide few insights into the mechanisms by which ultrasound induces the sustained modification to neuronal excitability and neural circuit function we and others have reported³⁴⁻³⁶.

In the present study, we investigate the mechanisms that underly ultrasound-induced modulation of neuronal action potential kinetics. We find that transient ultrasound exposure induces sustained, but reversible, modulation of whole-cell potassium current magnitude. Conversely, we observe no difference in whole-cell sodium currents between sham- and ultrasound-exposed neurons. A follow-up proteomics analysis indicates no change to total potassium channel abundance following ultrasound exposure but does suggest induction of $K_v2.1$ -specific dephosphorylation. Furthermore, Ingenuity Pathway Analysis indicates activation of synaptic signalling cascades. This is substantiated by miniature excitatory postsynaptic current (mEPSC) data demonstrating increased frequency of excitatory synaptic

transmission. Crucially, we find that the ultrasound-induced modulation of neuronal K_v channel function requires ionotropic glutamate receptor (AMPA/NMDAR) activation. Together, these results suggest specific patterns of pulsed ultrasound can induce a synaptic mechanism that drives modulation of neuronal excitability.

Results

Ultrasound induces sustained, reversible increases in whole-cell potassium currents.

We previously observed modified action potential kinetics, that persisted >12hrs, in neurons exposed to ultrasound³⁷. Voltage-gated potassium channels are the principal molecular components of action potential repolarisation. We therefore sought to assess the effect of ultrasound exposure on whole-cell potassium currents in the hours following stimulation. To do so, we first subjected primary rat cortical neurons to a 40 second, 200kHz pulsed ultrasound- or sham-treatment³⁷ (**Fig. 1A&B**; see methods). Subsequently, neurons were either transferred immediately to a recording chamber for electrophysiological analysis, or returned to the incubator for 6-, 12-, or 24-hours prior to assaying. Whole-cell potassium currents were recorded in voltage clamp mode in the presence of Na^+ and Ca^{2+} channel blockers (1 μ M TTX, 0.3mM $CdCl_2$). Neurons were voltage clamped at -70mV and currents were evoked by sequential 500ms voltage steps ranging from -70 to +80mV in 10mV increments. In neurons assayed within 0 – 2 hours of exposure, incremental voltage steps evoked progressively increasing current responses (**Fig. 1Ci&ii**). Compared to sham-treated neurons, ultrasound exposed neurons displayed a statistically significant ~25% increase in whole-cell current magnitude at +60mV ($p = 0.046$), +70mV ($p = 0.013$), and +80mV ($p = 0.004$), suggesting modulation of whole-cell potassium currents arising from modification of neuronal K_v channel function (**Fig. 1Cii**). There were no significant differences in voltage of half-maximal activation (**Fig. 1Ciii**) or slope of the I -V curve (**Fig. 1Civ**) indicating the voltage-dependence of K_v channel activation and conductance remains relatively unchanged.

We observed a similar effect on neurons assayed 6 – 8 hours following sham or ultrasound exposure (**Fig. 1D**). Whole-cell current magnitude was significantly increased by ~20% at +60mV ($p = 0.032$), +70mV ($p = 0.006$), and +80mV ($p = 0.001$), indicating the effect of ultrasound on K_v channel function persists well beyond the exposure period (**Fig. 1Dii**). This ultrasound induced increase in potassium current remained apparent at 12 – 14 hours following exposure (**Fig. 1E**). Once again, whole-cell currents were significantly increased in ultrasound exposed cells by ~25% at +60mV ($p = 0.014$), +70mV ($p = 0.003$) and +80mV ($p = 0.0007$), (**Fig. 1Eii**). Importantly, by 24-hours there was no significant differences in whole-cell potassium current magnitude between sham and ultrasound conditions at any voltage (**Fig. 1Fi&ii**), demonstrating the reversibility of the effects. When comparing across the time-course we found a significant effect of ultrasound on the maximum evoked current amplitude (**Fig. 1G**; effect of ultrasound: $F(1, 83) = 7.65, p = 0.007$; effect of time: $F(3, 83) = 2.01, p = 0.12$; effect of ultrasound x time interaction: $F(3, 83) = 2.40, p = 0.073$). There were no significant differences in voltage of half-maximal activation or slope of the I-V curve at 6 – 8 hours, 12 – 14 hours, or 24-hours following exposure (**Fig. 1D-Fiii&iv**), and no significant effects across the time-course (**Fig. 1H&I**), suggesting no effect of ultrasound exposure on the voltage-dependence of K_v channel function. Taken together these results indicate ultrasound exposure induces sustained, but reversible, increases in the magnitude of whole-cell potassium currents in cultured cortical rat neurons. These increases are apparent a few minutes after exposure, persist for at least 14 hours, and return to basal levels by 24 hours.

Ultrasound has no effect on whole-cell sodium currents.

Just as K_v channels drive action potential repolarisation, voltage-gated sodium channels (Na_v) are the primary mediators of action potential depolarisation. As such, functional changes in Na_v may also contribute to altered action potential kinetics. We therefore sought to determine whether ultrasound exposure had any lasting consequences for whole-cell sodium currents. We employed the same time-course paradigm, and whole-cell sodium currents were recorded in the presence of K^+ and Ca^{2+} channel blockers (30mM TEA-chloride, 1mM 4-AP, 0.3mM

CdCl₂). Neurons were voltage clamped at -70mV and currents were evoked by 25ms voltage steps ranging from -80 to +60mV in 10mV increments. In contrast to the observed effects on potassium currents, we observed no significant changes to whole-cell sodium current magnitude 0 – 2 hours following exposure (**Fig. 2Ai&ii**). In addition, there was no significant difference in the voltage of maximal activation (**Fig. 2Aiii**) or area under the curve (A.U.C., **Fig. 2Aiv**). This suggests that ultrasound has no effect on sodium current magnitude, activation voltage or total charge transfer immediately following exposure. Similarly, we observed no effect of ultrasound on sodium current magnitude across all voltage steps at 6 – 8 hours (**Fig. 2Bi&ii**), 12 – 14 hours (**Fig. 2Ci&ii**), or 24-hours following exposure (**Fig. 2Di&ii**). Again, there were no significant differences in voltage of maximal activation or maximum A.U.C. at any of these timepoints (**Fig. 2B-Diii&iv**), and there were no significant effects when comparing across the time-course (**Fig. 2E-G**). Together the data indicate ultrasound exposure has no immediate or lasting effects on Na_v channel function, implicating K_v channels as the primary target of ultrasound-induced neuronal excitability modifications.

Ultrasound does not alter voltage-gated ion channel abundance but may confer differential phosphorylation states.

Previous studies have demonstrated that K_v channel expression changes regulate K⁺ current magnitude and action potential kinetics^{42,43}. Additionally, differential phosphorylation of K_v subunits yields significant effects on channel function⁴⁴. Given the speed with which the effects on K_v channel function manifest (minutes), these are more likely a result of post-translational modifications than protein expression level changes. The duration of the effects (hours), however, might depend on altered protein expression. Accordingly, we sought to determine whether the observed changes to whole-cell potassium currents could be explained by changes to K_v channel expression or phosphorylation state. To do so, we initiated a tandem mass tag (TMT) nanoLC-MS/MS-based proteomic analysis of cortical neuron cultures (**Fig.3A**). Neuronal cultures derived from five animals were subjected to either sham or

ultrasound treatment. Cell lysates were harvested 2-hours post stimulation, yielding five sets of paired samples for proteomic analysis.

A total of 6194 proteins were identified in our samples, of those, only 4 (0.06%) were not identified in all the 10 individual samples (**Fig. 3B**). We identified significant upregulation of 328 proteins, and downregulation of 120 proteins, in the ultrasound exposed group. This equates to 7% of identified proteins being differentially expressed. In addition to total protein abundance, we also analysed phosphopeptide abundances (**Fig. 3C**). A total of 3314 individual phosphopeptides could be identified. Of these, 2997 (90%) could be reliably assigned to a protein target identified in the total protein abundance analysis, and 2961 (89%) were present in all 10 samples. As multiple distinct phosphopeptides may be derived from the same protein, this equated to 1192 specific protein targets for which phosphopeptide data was obtained. Of these 1192, we identified 52 protein targets with significantly upregulated phosphopeptides, and 30 protein targets with significantly downregulated phosphopeptides. This equates to approximately 7% of identified phosphoproteins exhibiting differential expression between sham and ultrasound groups.

To specifically investigate changes that may relate to our electrophysiology data, we searched the dataset for peptides assigned to voltage-gated ion channels (**Fig. 3D**). We identified 6 Na_v subunits. In accordance with our electrophysiology data, none of these were differentially expressed. We additionally identified 6 K_v subunits and none of these were differentially expressed either, suggesting the observed changes to whole-cell potassium currents are not driven by differences in total channel abundance. We did, however, identify a phosphopeptide associated with K_v2.1 which did display a marginally significant 1.15-fold downregulation in ultrasound treated neurons ($p = 0.048$). This may indicate the observed electrophysiological changes are driven by differential phosphorylation of a specific population of voltage-gated potassium channels.

Ultrasound induces functional increases in excitatory synaptic transmission.

To establish a more comprehensive overview of the intracellular signalling processes that may be regulated by ultrasound exposure, we performed Ingenuity Pathway Analysis⁴⁵ on the proteomics dataset. Analysis of canonical signalling pathways revealed 32 pathways that were significantly modulated by ultrasound with the number of associated proteins ranging from 3 – 18 (**Fig. 4A**). Strikingly, “synaptogenesis signalling pathway” was the most significantly modulated pathway ($p = 3 \times 10^{-6}$, $Z = 1.21$) with 18 associated proteins that displayed differential phosphorylation states between conditions. Associated proteins included kinases such as CaMKII α , CaMKII β and GSK3 β , receptors such as mGlu5, as well as MAP1B, Tau, Synapsin 1 & 2, and Synaptotagmin. This suggests brief ultrasound treatment induces synaptogenic signalling pathways within 2-hours of exposure.

Next, we sought to confirm whether ultrasound exposure is indeed inducing synaptogenesis by performing a high resolution, quantitative confocal immunofluorescence imaging experiment. Following sham or ultrasound exposure, neurons were fixed and immunostained for MAP2, Synapsin, and PSD-95, serving as neuronal morphology, pre-synapse and post-synapse markers, respectively (**Fig. 4B**). We performed synapse quantification 6hrs following sham or ultrasound exposure, given previous studies demonstrating quantifiable changes in synapse number between 2- and 72-hours following electrical or pharmacological intervention^{46–48}. Given that the proteomics data indicated differential phosphorylation of relevant kinases and receptors 2hrs after ultrasound exposure, we opted to delay synapse quantification for an additional 4hrs in order for the necessary structural reorganisation to occur at the subcellular level for functional synapses to be generated. Synapses were defined as colocalised Synapsin- and PSD-95-positive puncta located along MAP2-positive dendrites. A semi-automated analysis method was employed to quantify synapse density and size. We found no difference in synapse density (**Fig. 4C**), or puncta size (**Fig. 4D**), between sham- and ultrasound-exposed neurons, suggesting that, whilst synaptogenesis signalling may be

activated, this does not lead to structural changes in the number or size of synapses within this timeframe. Conversely, this may indicate that the differential phosphorylation of the proteins associated with “synaptogenesis signalling pathway”, is not in fact contributing to development of new synapses in this case and instead has other physiological consequences.

Although synaptogenesis *per se* was not apparent, many of the differentially regulated proteins associated with “synaptogenesis signalling” are also associated with regulation of synaptic transmission. We therefore tested whether ultrasound exposure induced functional changes to synaptic neurotransmission in cultured neurons by assaying miniature excitatory postsynaptic currents (mEPSC) within 0 – 2 hours following sham or ultrasound treatment (**Fig. 4E-G**). To measure mEPSCs, neurons were voltage-clamped at -60mV and current responses were recorded in the presence of tetrodotoxin (500nM TTX). We found that the frequency of mEPSCs was increased by 243% in ultrasound exposed neurons (**Fig. 4F**; $p = 2.5 \times 10^{-6}$). Conversely, we found no significant differences in the amplitude of mEPSCs (**Fig. 4G**). The substantially increased frequency of mEPSCs in ultrasound exposed neurons suggests ultrasound induces plasticity at excitatory synapses, enhancing excitatory synaptic transmission in the cultured neurons. In conjunction with the proteomics data, this suggests ultrasound stimulates synaptic intracellular signalling cascades that elicit functional changes to intercellular neurotransmission.

Ultrasound-induced modulation of voltage-gated potassium channel function is mediated via glutamatergic synapses.

Synaptic and intrinsic plasticity are known to occur in conjunction with one another⁴⁹. For instance, induction of the long-term potentiation (LTP) form of synaptic plasticity has been demonstrated to drive increases in intrinsic excitability⁵⁰. We therefore sought to establish whether ultrasound's effects on excitatory synaptic transmission and K_v channel function are causally linked. To do so, neurons were sham or ultrasound exposed in the presence of AP5

and NBQX to block, respectively, AMPA and NMDA receptor activation. We hypothesised that inhibition of glutamatergic receptor function would block the ultrasound-mediated enhancement of K^+ current magnitude. Neurons were pre-treated with the NMDA receptor antagonist AP5 (50 μ M) and AMPA receptor antagonist NBQX (10 μ M) prior to ultrasound exposure. Receptor antagonism was maintained during exposure and for 5 mins after. AP5 and NBQX were then removed and K_v channel function was assayed as described above.

Reproducing our previous results, in vehicle-treated neurons we observed a significant increase in K^+ current amplitude in ultrasound exposed neurons compared to sham at 60 – 80 mV (**Fig. 4H&I**: +60mV, $p = 0.016$; +70mV, $p = 0.0008$, +80mV, $p < 0.0001$). Importantly, in sham-exposed neurons we observed no significant difference between neurons pre-treated with AP5/NBQX or vehicle. This indicates AMPA/NMDA receptor antagonism *per se* does not modulate K_v channel function. Strikingly, when neurons were exposed to ultrasound in the presence of AP5/NBQX, the ultrasound-mediated enhancement was completely eliminated, measured as significant differences at 50 – 80 mV (+50mV, $p = 0.042$; +60mV, $p = 0.001$; +70mV, $p < 0.0001$; +80mV, $p < 0.00001$) compared with vehicle treated, ultrasound exposed neurons. There were no significant differences between either group of sham neurons or ultrasound exposed neurons treated with AP5/NBQX. Together the data indicate ionotropic glutamate receptor activation is required for ultrasound-induced modulation of K_v channel function.

Discussion

Voltage-gated Na^+ (Na_v) and K^+ (K_v) channels are the principal components of action potential generation and as such represent important targets for regulation of neuronal excitability. Indeed, altered neuronal excitability is directly linked with the modulation of voltage-gated ion channels^{51,52}. We previously reported sustained, reversible increases in neuronal excitability induced by ultrasound that occurred in conjunction with modified action potential kinetics³⁷.

We therefore sought to determine whether modulation of voltage-gated ion channel function may underpin these observations. Under the same conditions as our previous report, we observed sustained, reversible modulation of whole-cell K^+ , but not Na^+ , current magnitude by ultrasound, with comparable temporal characteristics. Previous studies have demonstrated ultrasound-induced modulation of both Na^+ and K^+ currents in hippocampal neurons^{40,41}. However, these modulations were observed during the ultrasound exposure period, in contrast to our report in which modulation is sustained following exposure.

Our proteomics analysis found no differences in total ion channel abundance following ultrasound treatment. We did identify dephosphorylation of the $K_v2.1$ channel at S563 in ultrasound exposed neurons, however, we were unable to validate this finding through immunoassays due to a lack of commercially available antibodies validated against this specific phosphosite and the findings should therefore be interpreted with caution. $K_v2.1$ has previously been shown to play a major role in action potential repolarisation and frequency-dependent regulation of excitability in rat hippocampal and cortical neurons^{42,53,54}. Additionally, S563 dephosphorylation has been shown to lead to faster activation and inactivation kinetics under whole-cell voltage clamp analysis⁴⁴. However, whether or not the modest 1.15-fold dephosphorylation of $K_v2.1$ we observe is sufficient to account for the ~25% increase in K^+ current magnitude is unclear and might suggest additional mechanisms are at play. What remains to be elucidated are the intracellular signalling cascades regulated by ultrasound and responsible for inducing longer-term changes to neuronal excitability which may be encoded through phosphorylation changes to specific ion channel subunits.

Our observations of sustained but reversible modification of neuronal excitability and K_v channel function is suggestive of plastic modification to intrinsic excitability. Whilst the dynamics of neural circuitry is often considered to rely primarily on synaptic modifications, evidence suggests that transient, patterned neuronal stimulation can rapidly modify intrinsic

excitability, regulated by changes to ion channel function⁵⁵. As such, it is becoming increasingly clear that activity-dependent modification of synaptic and excitability properties likely co-occur⁵⁶ and this is corroborated by the observations reported here. Our proteomic analysis suggests the induction of synaptogenic signalling in the cortical neuron cultures following ultrasound exposure. We did not, however, detect any differences in synapse density or size. One possible explanation is that the 6hrs following treatment (at which timepoint synapses were quantified) was insufficient time for the necessary protein synthesis, trafficking and structural reorganisation required for quantifiable changes in the number of synapses to occur. Previous studies have, for instance, quantified changes in synapse density 24hrs or more following pharmacological treatments^{47,48}. Conversely, given that the proteomics data indicates activation of synaptogenic signalling 2hrs following ultrasound exposure, it is possible that new synapses were generated but in the subsequent 4hrs these were lost and synapse density reverted to pre-treatment levels. For instance, previous reports have observed synaptogenesis in P15 rat hippocampal slices 2hrs after LTP induction, indicating synaptogenesis can be observed within similar timeframes⁵⁷. However, these were noted to be 'silent' synapses, and it is known that lack of stabilisation through functional integration of new spines can lead to their elimination⁵⁸. If this is the case, the functional relevance of these short-lived, silent synapses is likely to be limited.

Alternatively, these conflicting observations may be attributable to the publication-biased nature of proteomic pathway analyses. The 18 differentially regulated protein targets included in the "synaptogenesis signalling pathway", whilst known to play roles in synaptogenesis, also have important roles in many other aspects of synaptic function and signalling, and as such their regulation may have physiological consequences besides synaptogenesis in this instance. In support of this notion, we observed functional changes to synaptic electrophysiology amounting to substantial increases in the frequency of spontaneous excitatory synaptic transmission. Accordingly, the differential regulation of synaptic proteins

may have contributed to these observations. Collectively, these findings suggest specifically patterned ultrasound stimulation can elicit concurrent modification to neuronal excitability and synaptic function. Furthermore, we observed that inhibition of AMPA- and NMDA-receptor function prevents the ultrasound-induced increases in whole-cell K⁺ current magnitude, demonstrating a causal association between glutamatergic synaptic transmission and ultrasound-induced modulation of neuronal excitability. Previous work has demonstrated a role for both AMPA⁵⁹ and NMDA⁶⁰ receptors in the regulation of intrinsic excitability, providing avenues for future exploration of these mechanistic pathways regulated by ultrasound stimulation.

The ultrasound delivery protocol we employed involved a 200kHz carrier frequency delivered in 100ms pulses, with 100ms pulse intervals, for 40s, equating to a pulse repetition frequency of 5Hz. These parameters are similar to those of recent *in vivo* studies, conducted in non-human primates, demonstrating target-specific, bidirectional changes to functional connectivity that persist for hours beyond the stimulation period^{34,35}. These persistent changes to neuronal network activity, often termed “offline” effects, are indicative of plasticity induction by FUS. Interestingly, the 5Hz pulse repetition frequency employed here is analogous to electrical theta-burst stimulation (TBS) patterns originally used to induce plasticity in animal brain slices having been demonstrated to reliably induce LTP^{61,62}. Since those discoveries, TBS has been utilised in TMS studies *in vivo* to modulate cortical and corticospinal excitability⁶³, manipulate cognitive functions^{64,65}, and as a potential treatment for psychiatric disease^{66,67}. Indeed, TBS has been demonstrated to modulate hippocampal neuron excitability and potassium channel function analogous to the findings reported here⁶⁸. Recent studies in humans³⁶ and non-human primates⁶⁹ have demonstrated TBS-patterned FUS induces motor cortex excitability increases that can persist for at least 30 minutes following stimulation. Additionally, a recent report has demonstrated FUS-induced synaptic plasticity *in vivo* in rodents⁷¹. Together with our findings, this suggests specific pulsing frequencies, particularly

within the theta range, endow ultrasound with the capacity for plasticity induction, inducing both synaptic and intrinsic plasticity.

It is important to acknowledge some limitations; firstly, the glass coverslip we use acts as an acoustically hard reflector and hence changes the local intensity in the vicinity of the cells relative to *in vivo*. In the *in vivo* case the radiation force arises mainly from absorption, whereas *in vitro* (on the coverslip) there is an additional gradient forcing effect. At present the relative importance of these contributions is not known. Secondly, we performed finite-element modelling of the acoustic pressure field generated in our ultrasound stimulation system and found that we are likely establishing standing waves. This is estimated to result in a 2- to 4-fold increase in the pressure at the coverslip surface relative to the free-field pressure when varying the transducer-to-coverslip distance by 10mm (**Fig. S1**: 0.12MPa vs 0.2 – 0.39MPa). Whilst the 10mm range is higher than the variability in our experimental set-up, this suggests the pressures experienced by the neurons may have varied between experiments. Importantly, these pressures are still in line with those used *in vivo* in previous studies in humans and non-human primates^{3,4,5,9}. In addition, most common transcranial ultrasound methods use wavefields that are focused, and it is with noting that these also have pressure gradients which are fixed in space. If the higher pressure gradients experienced by the tissue in this paper are significant, then future *in vivo* experiment could be designed to replicate this type of field. This would mean the use of high numerical aperture focusing or multiple convergent beams.

More work is required to understand the mechanisms by which ultrasound induces synaptic plasticity and glutamate receptor-dependent excitability modifications, but our findings provide insights into the specific molecular and cellular components regulated by ultrasound that may underlie the persistent effects of FUS on neural circuit dynamics *in vivo*. Empirical evidence for an interesting novel mechanism for neuronal excitation by ultrasound was recently reported, involving calcium influx via mechanosensitive TRP channels leading to neuronal

depolarization initiated by calcium-mediated activation of TRPM4 and T-type Ca^{2+} channels⁷². Our findings implicate modification of K_v channel function, modulation of ionotropic glutamate receptor signalling, and activation of synaptic signalling cascades in response to ultrasound exposure. Given the scope for involvement of calcium-mediated signalling in our findings, this provides a tantalizing avenue for future research to identify a unifying mechanism for the immediate and sustained neuronal responses to ultrasound stimulation.

Conclusion

Transcranial ultrasound stimulation is rightfully garnering evermore attention as a potentially game-changing modality in the field of brain stimulation. However, understanding the longer-term effects of ultrasound stimulation on neuronal function will be tremendously important for two reasons: firstly, to provide confidence in the safety of the technique and secondly, to promote considered design of stimulation protocols to evoke particular molecular consequences and elicit specific effects on neural circuit dynamics. Together, this will advance the utility of FUS for both basic research and therapeutic applications. Our findings provide evidence of the capacity for ultrasound stimulation to induce plasticity of ion channels and synapses. These findings can inform the experimental design of future investigations employing FUS.

Methods

Primary rat cortical neuronal cultures. All animal experiments were carried out in accordance with the UK Scientific Procedures Act, 1986 and associated guidelines. The methods were carried out in accordance with the approved guidelines. All experimental protocols were approved by the University of Bristol Animal Welfare & Ethical Review Body. Cortical neurons are cultured from post-natal day 0 Wistar rats, in accordance with established methodology⁷³. Briefly, following Schedule 1 killing of the animal, the brain is removed and transferred to HABG media (HibernateA, B-27 Supplement and Glutamax) before dissection. Cortical tissue is then pulled apart into approximately 2mm^3 sections, then digested with

Trypsin-EDTA. Neurons are isolated using a Density Gradient Medium (OptiPrep), and finally plated onto 13mm diameter glass poly-D-lysine-coated coverslips at a density of 3×10^4 per cm^2 in NeurobasalA media (NeurobasalA, B-27 Supplement, Glutamax and Gentamicin). Cultures were maintained at 20% O_2 , 5% CO_2 , at 37°C .

Ultrasound exposure. Ultrasound delivery was conducted as described in Ref³⁷. Briefly, neurons were transferred to a chamber and submerged in HBS. A 200kHz ultrasound transducer (MCUSD19A200B11RS, Farnell, UK) powered by a signal generator (AFG3022B, Tektronix, USA) amplified by a radio frequency amplifier (25A250, Amplifier Research, USA), was used to generate the ultrasound stimulus. The transducer was excited with a 200kHz sinusoidal wave of amplitude 50V peak-to-peak, delivered in 100ms pulses at 100ms intervals, for 40 seconds, equating to a pulse repetition frequency of 5Hz. Control, sham exposure involved same procedure of cells being placed in the stimulation chamber for equal time, with all equipment powered on, but no excitation signal delivered to the transducer and thus no generation of ultrasound. Following treatment, cells were transferred to a recording chamber for electrophysiological analysis. To model the acoustic pressure field in our system we used a multi-physics finite element model (COMSOL Multiphysics 5.5). This modelled the transducer as a piezoelectric material using the electrostatics and solid mechanics interfaces and the other components using the pressure acoustics interface. Displacements and pressures were used to ensure continuity between these domains. The approach involves discretising the objects into small regions, or elements. The largest element size used was 1/15th of a wavelength which is smaller than the normal rule of 1/10th of a wavelength for finite element model convergence. In this model the wavelength in the water was 7.5mm and the largest element size was 0.5mm. The system was modelled as axis-symmetric which significantly reduced computation time relative to a fully 3D model. Various of the boundaries were set as radiating to further reduce the size of the modelled domain. Any waves reaching these boundaries are lost from the model, simulating a much larger domain. The resulting model was then run in the frequency domain, i.e., at 200kHz, by exciting a 50V sinusoidal

potential difference across the surfaces of the piezoelectric material. The stand-off distance from the transducer to the coverslip was varied from 4.5mm to 5.5mm and this caused the pressure at the surface of the glass to vary. The pressure increased from 0.2MPa when the stand-off distance was 4.5mm, reached a peak of 0.39MPa when the stand-off was 5mm and then decreased to 0.2MPa when the stand-off was 5.5mm. Hence in positioning the transducer at 5mm pressure within the petri dish was maximised.

Electrophysiology. Conventional whole-cell patch clamp recording is used in accordance with our established protocols⁷⁴. All recordings are made from primary cultured neurons at DIV 21 – 30. Following ultrasound or sham-stimulation, coverslips with plated neurons were placed in a recording chamber submerged in external recording solution (21-23°C) containing (in mM): 119 NaCl, 5 KCl, 25 HEPES, 33 glucose, 2 CaCl₂, 2 MgCl₂, 0.001 glycine, 0.1 picrotoxin, pH 7.4 adjusted with NaOH, flowing at 2ml/min. Recordings were made using an Axon Axopatch 200B Microelectrode Amplifier (Axon Instruments, Foster City, Canada). Signals were low-pass filtered at 5kHz and digitized at 20kHz. Glass microelectrodes were pulled by a micropipette puller P1000 (Sutter Instrument, Novato, California, USA) with resistances ranging from 4 to 8 MΩ after filling with internal solution. When recording isolated K⁺ and Na⁺ currents, capacitive currents were subtracted online, and series resistance (R_s) was compensated 75 – 85%. Only recordings where R_s was maintained <25 MOhm and membrane resistance (R_m) >100 MOhm were included. For K⁺ current recordings the internal solution contained (in mM): 135 K-gluconate, 10 HEPES, 8 NaCl, 0.5 EGTA, 2 Mg-ATP, 0.3 Na-GTP, pH 7.2 adjusted with KOH, osmolarity 285 mOsm. Neurons were voltage clamped at -70mV and subjected to 500ms depolarizing voltage steps from -70mV to +80mV in 10mV increments. Tetrodotoxin citrate (TTX - 1 μM - HelloBio #HB1035) and CdCl₂ (0.3 mM) were added to block sodium currents, Ca²⁺ current and Ca²⁺-dependent K⁺ currents. For Na⁺ current recordings the internal solution contained (in mM): 130 CsMeSO₄, 8 NaCl, 4 Mg-ATP, 0.3 Na-GTP, 0.5 EGTA, 10 HEPES, pH 7.2 adjusted with NaOH, osmolarity 280 mOsm. Neurons were voltage clamped at -70mV and subjected to 25ms depolarizing voltage steps from -80mV

to +60mV in 10mV increments. TEA-chloride (30 mM), 4-AP (1 μ M), and CdCl₂ (0.3 mM) were added to block Ca²⁺ current and Ca²⁺-dependent K⁺ currents. Evoked currents could be blocked by addition of 1 μ M TTX. For mEPSC recordings the internal solution was the same as Na⁺ current experiments with the addition of 6 mM QX-314 chloride. Neurons were voltage clamped at -60mV. During recordings, neurons were perfused with external solution containing 0.5 μ M TTX. Recordings were made for 6 minutes and the last 1-minute segment was analysed. The amplitude threshold for mEPSC detection was 12pA. Data was monitored online and saved using WinLTP v2.32⁷⁵ and later analysed offline using Clampfit (Molecular Devices, USA) software.

Quantitative proteomics.

Sample preparation: Coverslip plated neurons received either sham or ultrasound stimulation and were then incubated for 2 hours at 37°C with fresh media. Five coverslips from a culture derived from a single animal were used to generate one protein sample and another five from the same culture were used to generate the complimentary paired sample. This process was repeated using cultures from five separate animals yielding five sets of independently prepared paired samples (10 protein samples, 5 sham & 5 ultrasound, from 5 animals). Coverslips were washed twice with ice cold PBS and kept on ice. Cells were lysed in RIPA buffer (50 mM Tris pH 7.4, 150 mM NaCl, 1% Triton, 0.1% SDS, 1mM EDTA) with protease inhibitor cocktail at 1:10 [Roche 05892791001], serine/cysteine protease inhibitor phenylmethanesulfonyl fluoride (PMSF) (ThermoFisher, #P7626) at 1:100 and phosphatase inhibitor cocktail at 1:100 (ThermoFisher, #P5726). Cells were scraped with a pipette tip and the lysis buffer collected. samples were rotated at 25rpm at 4°C for 30 minutes. Samples were then centrifuged at 15000 x g for 10 minutes at 4°C and the supernatant collected. Protein was quantified using a BCA Protein Assay Kit, (ThermoFisher, #23225) and iMark Microplate Reader (Bio-Rad, California, USA).

TMT Labelling, High pH reversed-phase chromatography and Phospho-peptide enrichment:

Aliquots of 100µg of each sample were digested with trypsin (2.5µg trypsin per 100µg protein; 37°C, 16hrs), labelled with Tandem Mass Tag (TMT) ten plex reagents according to the manufacturer's protocol (Thermo Fisher Scientific, Loughborough, LE11 5RG, UK) and the labelled samples pooled.

For the Total proteome analysis, an aliquot of 50ug of the pooled sample was desalted using a SepPak cartridge according to the manufacturer's instructions (Waters, Milford, Massachusetts, USA). Eluate from the SepPak cartridge was evaporated to dryness and resuspended in buffer A (20 mM ammonium hydroxide, pH 10) prior to fractionation by high pH reversed-phase chromatography using an Ultimate 3000 liquid chromatography system (Thermo Fisher Scientific). In brief, the sample was loaded onto an XBridge BEH C18 Column (130Å, 3.5 µm, 2.1 mm X 150 mm, Waters, UK) in buffer A and peptides eluted with an increasing gradient of buffer B (20 mM ammonium hydroxide in acetonitrile, pH 10) from 0-95% over 60 minutes. The resulting fractions (15 in total) were evaporated to dryness and resuspended in 1% formic acid prior to analysis by nano-LC MSMS using an Orbitrap Fusion Lumos mass spectrometer (Thermo Scientific).

For the phospho proteome analysis, the remainder of the TMT-labelled pooled sample was also desalted using a SepPak cartridge (Waters, Milford, Massachusetts, USA). Eluate from the SepPak cartridge was evaporated to dryness and subjected to TiO₂-based phosphopeptide enrichment according to the manufacturer's instructions (Pierce). The flow-through and washes from the TiO₂-based enrichment were then subjected to FeNTA-based phosphopeptide enrichment according to the manufacturer's instructions (Pierce). The phospho-enriched samples were again evaporated to dryness and then resuspended in 1% formic acid prior to analysis by nano-LC MSMS using an Orbitrap Fusion Lumos mass spectrometer (Thermo Scientific).

Nano-LC Mass Spectrometry: High pH RP fractions (Total proteome analysis) or the phospho-enriched fractions (Phospho-proteome analysis) were further fractionated using an Ultimate 3000 nano-LC system in line with an Orbitrap Fusion Lumos mass spectrometer (Thermo Scientific). In brief, peptides in 1% (vol/vol) formic acid were injected onto an Acclaim PepMap C18 nano-trap column (Thermo Scientific). After washing with 0.5% (vol/vol) acetonitrile 0.1% (vol/vol) formic acid peptides were resolved on a 250 mm × 75 µm Acclaim PepMap C18 reverse phase analytical column (Thermo Scientific) over a 150 min organic gradient, using 7 gradient segments (1-6% solvent B over 1min., 6-15% B over 58min., 15-32%B over 58min., 32-40%B over 5min., 40-90%B over 1min., held at 90%B for 6min and then reduced to 1%B over 1min.) with a flow rate of 300 nl min⁻¹. Solvent A was 0.1% formic acid and Solvent B was aqueous 80% acetonitrile in 0.1% formic acid. Peptides were ionized by nano-electrospray ionization at 2.0kV using a stainless-steel emitter with an internal diameter of 30 µm (Thermo Scientific) and a capillary temperature of 300°C.

All spectra were acquired using an Orbitrap Fusion Lumos mass spectrometer controlled by Xcalibur 3.0 software (Thermo Scientific) and operated in data-dependent acquisition mode using an SPS-MS3 workflow. FTMS1 spectra were collected at a resolution of 120 000, with an automatic gain control (AGC) target of 200 000 and a max injection time of 50ms. Precursors were filtered with an intensity threshold of 5000, according to charge state (to include charge states 2-7) and with monoisotopic peak determination set to Peptide. Previously interrogated precursors were excluded using a dynamic window (60s +/-10ppm). The MS2 precursors were isolated with a quadrupole isolation window of 0.7m/z. ITMS2 spectra were collected with an AGC target of 10 000, max injection time of 70ms and CID collision energy of 35%.

For FTMS3 analysis, the Orbitrap was operated at 50 000 resolution with an AGC target of 50 000 and a max injection time of 105ms. Precursors were fragmented by high energy collision dissociation (HCD) at a normalised collision energy of 60% to ensure maximal TMT reporter

ion yield. Synchronous Precursor Selection (SPS) was enabled to include up to 10 MS2 fragment ions in the FTMS3 scan.

Data Analysis: The raw data files were processed and quantified using Proteome Discoverer software v2.1 (Thermo Scientific) and searched against the UniProt rat database (retrieved August 2021) using the SEQUEST HT algorithm. Peptide precursor mass tolerance was set at 10ppm, and MS/MS tolerance was set at 0.6Da. Search criteria included oxidation of methionine (+15.995Da), acetylation of the protein N-terminus (+42.011Da) and Methionine loss plus acetylation of the protein N-terminus (-89.03Da) as variable modifications and carbamidomethylation of cysteine (+57.0214) and the addition of the TMT mass tag (+229.163) to peptide N-termini and lysine as fixed modifications. For the Phospho-proteome analysis, phosphorylation of serine, threonine and tyrosine (+79.966) was also included as a variable modification. Searches were performed with full tryptic digestion and a maximum of 2 missed cleavages were allowed. The reverse database search option was enabled and all data was filtered to satisfy false discovery rate (FDR) of 5%. Statistical significance was then determined using paired T-Tests between the conditions of interest. The p-values were FDR corrected using the Benjamini-Hochberg method.

For pathway analysis the master protein accessions, phospho-site, and corresponding p-values, FDR-adjusted p-values and Log2 fold-changes were all uploaded to QIAGEN Ingenuity Pathway Analysis (IPA) software⁴⁵. A p-value cut-off of $p < 0.05$ applied to the expression (total protein) and phosphorylation core analyses. Canonical pathways analysis identified the pathways from the QIAGEN Ingenuity Pathway Analysis library of canonical pathways that were most significant to the data set. Molecules from the data set that met the p-value cut-off and were associated with a canonical pathway in the QIAGEN Knowledge Base were considered for the analysis. The significance of the association between the dataset target proteins and the canonical pathways are expressed as p-values derived by right-tailed Fisher's Exact Test.

Immunocytochemistry. Coverslip plated neurons were fixed in 4% paraformaldehyde 6hrs after sham or ultrasound treatment. Neurons were permeabilized in phosphate-buffered saline (PBS; 137mM NaCl, 2.7mM KCl, 10mM PO₄) with 0.1% Triton X-100 for 10 min at room temperature (RT, 20 – 22°C), and blocked in PBST (PBS + 0.1% Tween-20) with 1% bovine serum albumin (BSA) and 300mM glycine for 1 h at RT. Primary antibodies were diluted in 1% BSA in PBST and applied overnight at 4 °C. Secondary fluorophore-conjugated antibodies were diluted in 1% BSA in PBS and applied for 1 h at RT. Coverslips were mounted on glass slides using ProLong Glass Antifade Mountant (Invitrogen, P36980) and cured overnight. Primary antibodies used were chicken anti-MAP2 (Abcam, Cat# ab5392, 1:5000), mouse anti-PSD-95 (Abcam, Cat# ab192757, 1:250), and rabbit anti-Synapsin (Cell Signalling, Cat# 2312S, 1:250). Corresponding secondary antibodies were goat anti-chicken AlexaFluor 405 (Invitrogen, Cat# A48260, 1:200), goat anti-mouse AlexaFluor 555 (Invitrogen, Cat# A21424, 1:200), and goat anti-rabbit AlexaFluor 488 (Invitrogen, Cat# A11034, 1:200).

Synapse quantification. Images were acquired on a Leica DMI8 microscope with Leica SP8 AOBs confocal laser scanning system using 50mW 405nm diode, 65mW 488nm Argon, 20mW 561nm DPSS laser lines in conjunction with LAS X software v3.5.7.23225 (Leica Microsystems). Images were captured with a 1mm pinhole, 63x oil-immersion objective (numerical aperture 1.4) covering an area of 105.69 x 105.69 μm with pixel size of 58.72 nm and 2x line averaging. All images were acquired with standardised laser power and gain conditions. Five non-overlapping z-stacks containing six slices at 300nm intervals were captured per coverslip and four independent preparations, derived from four animals, were used per experimental condition. Image analysis was conducted in Fiji⁷⁶. Synapses were defined as colocalised presynaptic (Synapsin) and postsynaptic (PSD-95) puncta located along MAP2 positive dendrites. Following background subtraction, the neuronal soma was manually cleared. A 3 pixel maximum filter, and Huang2 thresholding was applied to the MAP2

channel to create a mask over the dendritic area. Presynaptic and postsynaptic channels were cleared outside the mask leaving only puncta located along dendrites. The automated Fiji plug-in Synapse Counter⁷⁷ was used for quantification of colocalised pre- and postsynaptic puncta. During quantification, settings for synapse counting were uniformly chosen for all images after optimisation on previously acquired images under the same conditions. Results of automatic puncta quantification were always validated by visual inspection and manual counting for a subset of images. All images were coded and processed in a blinded manner. Synapse density is expressed as the number of synapses per MAP2 positive dendrite area (measured from the thresholded mask area). Approximately 45,000 synapses were analysed per experimental condition.

Data analysis and statistics. After initial analyses in aforementioned software (Clampfit, Fiji, PD or IPA) resulting data was transported into GraphPad Prism (macOS v8.4.3, GraphPad Software, San Diego, California, USA), for statistical analysis and graphical representation. Data was tested for normality by D'Agostino and Pearson K2 test ($p < 0.01$). Where data was normally distributed, it has been presented as mean \pm S.E.M. (i.e., scatter dot plots), where it was not, data has been presented as median with inter-quartile range (i.e., box-and-whisker plots). Non-normal data was analysed by Mann-Whitney U test. Normally distributed data was analysed by either two-tailed unpaired t-test (with Holm-Sidak correction for multiple comparisons where applicable), two-tailed paired t-test, or 2-way analysis of variance (ANOVA), as indicated in the figure legends.

Data Availability

All source data that support the findings of this study are available from the corresponding author upon reasonable request.

References

1. Fomenko, A., Neudorfer, C., Dallapiazza, R. F., Kalia, S. K. & Lozano, A. M. Low-intensity ultrasound neuromodulation: An overview of mechanisms and emerging human applications. *Brain Stimulation* Preprint at <https://doi.org/10.1016/j.brs.2018.08.013> (2018).
2. Blackmore, J., Shrivastava, S., Sallet, J., Butler, C. R. & Cleveland, R. O. Ultrasound Neuromodulation: A Review of Results, Mechanisms and Safety. *Ultrasound Med Biol* **45**, 1509–1536 (2019).
3. Pouget, P. *et al.* Neuronavigated Repetitive Transcranial Ultrasound Stimulation Induces Long-Lasting and Reversible Effects on Oculomotor Performance in Non-human Primates. *Front Physiol* (2020) doi:10.3389/fphys.2020.01042.
4. Kubanek, J. *et al.* Remote, brain region–specific control of choice behavior with ultrasonic waves. *Sci Adv* **6**, eaaz4193 (2020).
5. Badran, B. W. *et al.* Sonication of the anterior thalamus with MRI-Guided transcranial focused ultrasound (tFUS) alters pain thresholds in healthy adults: A double-blind, sham-controlled study. *Brain Stimul* **13**, 1805–1812 (2020).
6. Nitsche, M. A. *et al.* Transcranial direct current stimulation: State of the art 2008. *Brain Stimul* **1**, 206–223 (2008).
7. Klomjai, W., Katz, R. & Lackmy-Vallée, A. Basic principles of transcranial magnetic stimulation (TMS) and repetitive TMS (rTMS). *Ann Phys Rehabil Med* **58**, 208–213 (2015).
8. Legon, W., Ai, L., Bansal, P. & Mueller, J. K. Neuromodulation with single-element transcranial focused ultrasound in human thalamus. *Hum Brain Mapp* **39**, 1995–2006 (2018).
9. Legon, W. *et al.* Transcranial focused ultrasound modulates the activity of primary somatosensory cortex in humans. *Nat Neurosci* **17**, 322–329 (2014).
10. Sanguinetti, J. L. *et al.* Transcranial Focused Ultrasound to the Right Prefrontal Cortex Improves Mood and Alters Functional Connectivity in Humans. *Front Hum Neurosci* (2020) doi:10.3389/fnhum.2020.00052.
11. Mueller, J., Legon, W., Opitz, A., Sato, T. F. & Tyler, W. J. Transcranial focused ultrasound modulates intrinsic and evoked EEG dynamics. *Brain Stimul* **7**, 900–908 (2014).
12. Lee, W. *et al.* Image-guided transcranial focused ultrasound stimulates human primary somatosensory cortex. *Sci Rep* **5**, 8743 (2015).
13. Dallapiazza, R. F. *et al.* Noninvasive neuromodulation and thalamic mapping with low-intensity focused ultrasound. *J Neurosurg* **128**, 875–884 (2018).
14. Ai, L., Bansal, P., Mueller, J. K. & Legon, W. Effects of transcranial focused ultrasound on human primary motor cortex using 7T fMRI: a pilot study. *BMC Neurosci* **19**, 56 (2018).
15. Legon, W., Bansal, P., Tyshynsky, R., Ai, L. & Mueller, J. K. Transcranial focused ultrasound neuromodulation of the human primary motor cortex. *Sci Rep* **8**, 10007 (2018).
16. Beisteiner, R. *et al.* Transcranial Pulse Stimulation with Ultrasound in Alzheimer’s Disease—A New Navigated Focal Brain Therapy. *Advanced Science* **7**, 1902583 (2020).

17. Ai, L., Mueller, J. K., Grant, A., Eryaman, Y. & Legon, W. Transcranial focused ultrasound for BOLD fMRI signal modulation in humans. *Annual International Conference of the IEEE Engineering in Medicine and Biology Society*. **2016**, 1758–1761 (2016).
18. Lee, W. *et al.* Transcranial focused ultrasound stimulation of human primary visual cortex. *Sci Rep* **6**, 34026 (2016).
19. Lee, W., Chung, Y. A., Jung, Y., Song, I.-U. & Yoo, S.-S. Simultaneous acoustic stimulation of human primary and secondary somatosensory cortices using transcranial focused ultrasound. *BMC Neurosci* **17**, 68 (2016).
20. Butler, C. R. *et al.* Transcranial ultrasound stimulation to human middle temporal complex improves visual motion detection and modulates electrophysiological responses. *Brain Stimulation: Basic, Translational, and Clinical Research in Neuromodulation* **15**, 1236–1245 (2022).
21. Yoon, K. *et al.* Effects of sonication parameters on transcranial focused ultrasound brain stimulation in an ovine model. *PLoS One* **14**, e0224311 (2019).
22. King, R. L., Brown, J. R. & Pauly, K. B. Localization of ultrasound-induced in vivo neurostimulation in the mouse model. *Ultrasound Med Biol* **40**, 1512–1522 (2014).
23. Oh, S.-J. *et al.* Ultrasonic Neuromodulation via Astrocytic TRPA1. *Curr Biol* **29**, 3386–3401.e8 (2019).
24. Bongioanni, A. *et al.* Activation and disruption of a neural mechanism for novel choice in monkeys. *Nature* **591**, 270–274 (2021).
25. Lee, K. S. *et al.* Focused Ultrasound Stimulation as a Neuromodulatory Tool for Parkinson’s Disease: A Scoping Review. *Brain Sciences* Preprint at <https://doi.org/10.3390/brainsci12020289> (2022).
26. Tyler, W. J. *et al.* Remote Excitation of Neuronal Circuits Using Low-Intensity, Low-Frequency Ultrasound. *PLoS One* **3**, e3511 (2008).
27. Lin, Z. *et al.* Ultrasound Stimulation Modulates Voltage-Gated Potassium Currents Associated With Action Potential Shape in Hippocampal CA1 Pyramidal Neurons. *Front Pharmacol* **10**, 544 (2019).
28. Weinreb, E. & Moses, E. Mechanistic insights into ultrasonic neurostimulation of disconnected neurons using single short pulses. *Brain Stimul* **15**, 769–779 (2022).
29. Tyler, W. J. *et al.* Remote Excitation of Neuronal Circuits Using Low-Intensity, Low-Frequency Ultrasound. *PLoS One* **3**, e3511 (2008).
30. Kubanek, J. *et al.* Ultrasound modulates ion channel currents. *Sci Rep* **6**, 24170 (2016).
31. Babakhanian, M. *et al.* Effects of Low Intensity Focused Ultrasound on Liposomes Containing Channel proteins. *Sci Rep* **8**, 17250 (2018).
32. Plaksin, M., Shoham, S. & Kimmel, E. Intramembrane Cavitation as a Predictive Bio-Piezoelectric Mechanism for Ultrasonic Brain Stimulation. *Phys Rev X* **4**, 11004 (2014).
33. Oh, S.-J. *et al.* Ultrasonic Neuromodulation via Astrocytic TRPA1. *Curr Biol* **29**, 3386–3401.e8 (2019).

34. Folloni, D. *et al.* Manipulation of Subcortical and Deep Cortical Activity in the Primate Brain Using Transcranial Focused Ultrasound Stimulation. *Neuron* **101**, 1109-1116 e5 (2019).
35. Verhagen, L. *et al.* Offline impact of transcranial focused ultrasound on cortical activation in primates. *Elife* **8**, (2019).
36. Zeng, K. *et al.* Induction of Human Motor Cortex Plasticity by Theta Burst Transcranial Ultrasound Stimulation. *Ann Neurol* **91**, 238–252 (2022).
37. Clennell, B. *et al.* Transient ultrasound stimulation has lasting effects on neuronal excitability. *Brain Stimulation: Basic, Translational, and Clinical Research in Neuromodulation* **14**, 217–225 (2021).
38. Kubanek, J. *et al.* Ultrasound modulates ion channel currents. *Sci Rep* **6**, 24170 (2016).
39. Tyler, W. J. *et al.* Remote excitation of neuronal circuits using low-intensity, low-frequency ultrasound. *PLoS One* **3**, e3511 (2008).
40. Lin, Z. *et al.* On-Chip Ultrasound Modulation of Pyramidal Neuronal Activity in Hippocampal Slices. *Adv Biosyst* (2018) doi:10.1002/adbi.201800041.
41. Lin, Z. *et al.* Ultrasound stimulation modulates voltage-gated potassium currents associated with action potential shape in hippocampal CA1 pyramidal neurons. *Front Pharmacol* (2019) doi:10.3389/fphar.2019.00544.
42. Du, J., Haak, L. L., Phillips-Tansey, E., Russell, J. T. & McBain, C. J. Frequency-dependent regulation of rat hippocampal somato-dendritic excitability by the K⁺ channel subunit Kv2.1. *Journal of Physiology* (2000) doi:10.1111/j.1469-7793.2000.t01-2-00019.xm.
43. Palacio, S. *et al.* Heterogeneity in Kv2 channel expression shapes action potential characteristics and firing patterns in CA1 versus CA2 hippocampal pyramidal neurons. *eNeuro* (2017) doi:10.1523/ENEURO.0267-17.2017.
44. Park, K. S., Mohapatra, D. P., Misonou, H. & Trimmer, J. S. Graded regulation of the Kv2.1 potassium channel by variable phosphorylation. *Science (1979)* (2006) doi:10.1126/science.1124254.
45. Krämer, A., Green, J., Pollard, J. & Tugendreich, S. Causal analysis approaches in ingenuity pathway analysis. *Bioinformatics* (2014) doi:10.1093/bioinformatics/btt703.
46. Harris, K. M. Structural LTP: from synaptogenesis to regulated synapse enlargement and clustering. *Curr Opin Neurobiol* **63**, 189–197 (2020).
47. Speranza, L. *et al.* Serotonin 5-HT₇ receptor increases the density of dendritic spines and facilitates synaptogenesis in forebrain neurons. *J Neurochem* **141**, 647–661 (2017).
48. Lee, J.-W. *et al.* Orphan GPR110 (ADGRF1) targeted by N-docosahexaenoyl ethanolamine in development of neurons and cognitive function. *Nat Commun* **7**, 13123 (2016).
49. Debanne, D., Inglebert, Y. & Russier, M. Plasticity of intrinsic neuronal excitability. *Current Opinion in Neurobiology* Preprint at <https://doi.org/10.1016/j.conb.2018.09.001> (2019).
50. Belmeguenai, A. *et al.* Intrinsic plasticity complements long-term potentiation in parallel fiber input gain control in cerebellar Purkinje cells. *J Neurosci* **30**, 13630–13643 (2010).

51. Fruscione, F. *et al.* PRRT2 controls neuronal excitability by negatively modulating Na⁺ channel 1.2/1.6 activity. *Brain* **141**, 1000–1016 (2018).
52. Campanac, E. *et al.* Enhanced intrinsic excitability in basket cells maintains excitatory-inhibitory balance in hippocampal circuits. *Neuron* **77**, 712–722 (2013).
53. Guan, D., Armstrong, W. E. & Foehring, R. C. Kv2 channels regulate firing rate in pyramidal neurons from rat sensorimotor cortex. *Journal of Physiology* (2013) doi:10.1113/jphysiol.2013.257253.
54. Liu, P. W. & Bean, B. P. Kv2 channel regulation of action potential repolarization and firing patterns in superior cervical ganglion neurons and hippocampal CA1 pyramidal neurons. *Journal of Neuroscience* (2014) doi:10.1523/JNEUROSCI.1925-13.2014.
55. Campanac, E. *et al.* Enhanced intrinsic excitability in basket cells maintains excitatory-inhibitory balance in hippocampal circuits. *Neuron* **77**, 712–722 (2013).
56. Belmeguenai, A. *et al.* Intrinsic plasticity complements long-term potentiation in parallel fiber input gain control in cerebellar Purkinje cells. *J Neurosci* **30**, 13630–13643 (2010).
57. Harris, K. M. Structural LTP: from synaptogenesis to regulated synapse enlargement and clustering. *Current Opinion in Neurobiology* Preprint at <https://doi.org/10.1016/j.conb.2020.04.009> (2020).
58. Berry, K. P. & Nedivi, E. Spine Dynamics: Are They All the Same? *Neuron* **96**, 43–55 (2017).
59. Dasgupta, D. & Sikdar, S. K. Calcium permeable AMPA receptor-dependent long lasting plasticity of intrinsic excitability in fast spiking interneurons of the dentate gyrus decreases inhibition in the granule cell layer. *Hippocampus* (2015) doi:10.1002/hipo.22371.
60. Hou, G. & Zhang, Z. W. NMDA receptors regulate the development of neuronal intrinsic excitability through cell-autonomous mechanisms. *Front Cell Neurosci* (2017) doi:10.3389/fncel.2017.00353.
61. Capocchi, G., Zampolini, M. & Larson, J. Theta burst stimulation is optimal for induction of LTP at both apical and basal dendritic synapses on hippocampal CA1 neurons. *Brain Res* (1992) doi:10.1016/0006-8993(92)91715-Q.
62. Larson, J. & Lynch, G. Induction of synaptic potentiation in hippocampus by patterned stimulation involves two events. *Science* (1979) (1986) doi:10.1126/science.3704635.
63. Suppa, A. *et al.* Ten Years of Theta Burst Stimulation in Humans: Established Knowledge, Unknowns and Prospects. *Brain Stimul* (2016) doi:10.1016/j.brs.2016.01.006.
64. Rounis, E., Maniscalco, B., Rothwell, J. C., Passingham, R. E. & Lau, H. Theta-burst transcranial magnetic stimulation to the prefrontal cortex impairs metacognitive visual awareness. *Cogn Neurosci* (2010) doi:10.1080/17588921003632529.
65. Gratton, C., Lee, T. G., Nomura, E. M. & D’Esposito, M. The effect of theta-burst TMS on cognitive control networks measured with resting state fMRI. *Front Syst Neurosci* (2013) doi:10.3389/fnsys.2013.00124.
66. Philip, N. S. *et al.* Theta-burst transcranial magnetic stimulation for posttraumatic stress disorder. *American Journal of Psychiatry* (2019) doi:10.1176/appi.ajp.2019.18101160.

67. Williams, N. R. *et al.* High-dose spaced theta-burst TMS as a rapid-acting antidepressant in highly refractory depression. *Brain* Preprint at <https://doi.org/10.1093/brain/awx379> (2018).
68. Fan, Y. *et al.* Activity-dependent decrease of excitability in rat hippocampal neurons through increases in Ih. *Nat Neurosci* (2005) doi:10.1038/nn1568.
69. Samuel, N. *et al.* Multi-modal investigation of transcranial ultrasound-induced neuroplasticity of the human motor cortex. *Brain Stimul* **15**, 1337–1347 (2022).
70. Niu, X., Yu, K. & He, B. Transcranial focused ultrasound induces sustained synaptic plasticity in rat hippocampus. *Brain Stimul* **15**, 352–359 (2022).
71. Yoo, S., Mittelstein, D. R., Hurt, R. C., Lacroix, J. & Shapiro, M. G. Focused ultrasound excites cortical neurons via mechanosensitive calcium accumulation and ion channel amplification. *Nat Commun* **13**, 493 (2022).
72. Brewer, G. J. & Torricelli, J. R. Isolation and culture of adult neurons and neurospheres. *Nat Protoc* **2**, 1490–1498 (2007).
73. Whitcomb, D. J. *et al.* Intracellular oligomeric amyloid-beta rapidly regulates GluA1 subunit of AMPA receptor in the hippocampus. *Sci Rep* **5**, (2015).
74. Anderson, W. W. & Collingridge, G. L. Capabilities of the WinLTP data acquisition program extending beyond basic LTP experimental functions. *J Neurosci Methods* **162**, 346–356 (2007).
75. Schindelin, J. *et al.* Fiji: An open-source platform for biological-image analysis. *Nature Methods* Preprint at <https://doi.org/10.1038/nmeth.2019> (2012).
76. Dzyubenko, E., Rozenberg, A., Hermann, D. M. & Faissner, A. Colocalization of synapse marker proteins evaluated by STED-microscopy reveals patterns of neuronal synapse distribution in vitro. *J Neurosci Methods* (2016) doi:10.1016/j.jneumeth.2016.09.001.

Acknowledgements

This work was completed with the support of the GW4 Alliance (GW4), Medical Research Council (MRC), and Bristol Research into Alzheimer's and Care for the Elderly (BRACE). This work was supported by Medical Research Council (MR/N0137941/1). The authors gratefully acknowledge the Wolfson Bioimaging Facility for their support and assistance in this work.

Competing Interests

The authors declare no competing interests.

Figure Legends

Figure 1: Ultrasound exposure induces increases whole-cell potassium current magnitude that persists up to 14-hours post-stimulation. (A) Schematic depicting ultrasound exposure paradigm involving coverslip plated primary rat neuronal cultures. Neurons are submerged in HBS and exposed to ultrasound from a distance of 0.5 cm, prior to electrophysiological analysis. (B) Schematic representing the ultrasound parameters. (C-F) Whole-cell potassium current data at four different time-points (C) 0 – 2 hours, (D) 6 – 8 hours, (E) 12 – 14 hours, and (F) 24 – 26 hours post-stimulation. Potassium currents are recorded in response to sequential voltage-steps from a holding potential of -70mV. In each panel: (i) Representative current responses to 500ms voltage steps recorded from sham (blue) and ultrasound (orange) stimulated cells (top), and 500ms voltage-step protocol from -70mV to +80mV in 10mV steps (bottom). (ii) I-V response curves derived from peak current magnitude, demonstrating whole-cell potassium currents were significantly increased in ultrasound stimulated neurons at 0 – 2 hours, 6 – 8 hours, and 12 – 14 hours, but returned to pre-stimulation levels by 24 – hours. Analysed by 2-tailed unpaired t-test with Holm-Sidak correction for multiple comparisons. (iii) Voltage of half-maximal activation (V_{50}) and (iv) I-V slope, derived from normalised I-V curves fit with Boltzmann sigmoid model, and were not significantly different at any timepoint. Analysed by 2-tailed unpaired t-test. Time-course summary data displaying significant effect of ultrasound exposure on (E) Maximum current response magnitude across the time-course (effect of ultrasound: $F(1, 83) = 7.65$, $p = 0.007$; effect of time: $F(3, 83) = 2.01$, $p = 0.119$; effect of ultrasound x time interaction: $F(3, 83) = 2.40$, $p = 0.073$), but not (F) V_{50} (effect of ultrasound: $F(1, 83) = 0.051$, $p = 0.82$; effect of time: $F(3, 83) = 2.49$, $p = 0.066$; effect of ultrasound x time interaction: $F(3, 83) = 0.526$, $p = 0.666$), and (G) I-V slope (effect of ultrasound: $F(1, 83) = 0.366$, $p = 0.547$; effect of time: $F(3, 83) = 0.269$, $p = 0.848$; effect of ultrasound x time interaction: $F(3, 83) = 1.89$, $p = 0.138$). Analysed by 2-way ANOVA. N = number of neurons and is indicated in (ii) for each timepoint. Data is mean \pm S.E.M. * $p < 0.05$, ** $p < 0.01$, *** $p < 0.001$

Figure 2: Ultrasound exposure has no post-stimulation effect on whole-cell sodium currents. (A-D) Whole-cell sodium current data at four different time-points (A) 0 – 2 hours, (B) 6 – 8 hours, (C) 12 – 14 hours, and (D) 24 – 26 hours post-exposure. Sodium currents are recorded in response to sequential voltage-steps from a holding potential of -80mV. In each panel: (i) Representative current responses to 500ms voltage steps recorded from sham (blue) and ultrasound (orange) exposed cells (top), and 500ms voltage-step protocol from -80mV to +60mV in 10mV steps (bottom). (ii) I-V response curves derived from peak current magnitude, demonstrating no effect of ultrasound on whole-cell sodium currents at any timepoint. Analysed by 2-tailed unpaired t-test with Holm-Sidak correction for multiple comparisons. (iii) Voltage of maximal activation (V_{100}) and (iv) area under the curve (A.U.C.), derived from current responses at the maximal activation voltage, were not significantly different at any timepoint. Analysed by 2-tailed unpaired t-test. Time-course summary data displaying no significant effect of ultrasound exposure on (E) Maximum current response magnitude across the time-course (effect of ultrasound: $F(1, 94) = 0.026$, $p = 0.871$; effect of time: $F(3, 94) = 0.780$, $p = 0.508$; effect of ultrasound x time interaction: $F(3, 94) = 0.97$, $p = 0.41$), (F) V_{100} (effect of ultrasound: $F(1, 94) = 0.277$, $p = 0.6$; effect of time: $F(3, 94) = 2.56$, $p = 0.060$; effect of ultrasound x time interaction: $F(3, 94) = 0.821$, $p = 0.486$), and (G) A.U.C. (effect of ultrasound: $F(1, 94) = 0.019$, $p = 0.891$; effect of time: $F(3, 94) = 0.44$, $p = 0.725$; effect of ultrasound x time interaction: $F(3, 94) = 0.579$, $p = 0.631$). Analysed by 2-way ANOVA. N = number of neurons and is indicated in (ii) for each timepoint. Data is mean \pm S.E.M.

Figure 3. Total- and phospho-proteome analysis indicates differential phosphorylation of K_v subunit. (A) Schematic depiction of proteomic workflow. Cell lysates are harvested from paired sister cultures subjected to either sham or ultrasound exposure. Protein samples are reduced, alkylated and digested, and resulting peptides are labelled with TMT tags. Samples are then pooled and 5% of the pooled samples are fractionated by high pH reverse-phase (RP) chromatography for total protein content analysis. The remaining 95% of the pool undergo phosphopeptide enrichment steps for analysis of phosphopeptides. Both sets of

samples are then analysed by nano-LC mass spectrometry and quantified using Proteome Discover software. Resulting quantitated data is used for pathway analysis using Ingenuity Pathway Analysis software. (B) Volcano plot displaying the log₂ fold change (x axis) against the t test–derived $-\log_{10}$ statistical P value (y axis) illustrating proteins differentially expressed between sham and ultrasound (US) exposed neuronal proteomes. Proteins significantly downregulated ($p < 0.05$) in US exposed neurons are shown in blue, and proteins significantly upregulated are displayed in red. The five proteins displaying the most significant or largest fold-changes are labelled. (C) Volcano plot displaying differential phosphoprotein expression with all axis and labelling same as in (A). (D) Dot plots comparing total protein abundance for specific Na_v (top, orange) and K_v (bottom, green) voltage-gated ion channel subunits taken from the dataset in (B). No significant differences were observed between sham and ultrasound exposed neurons. However, we did identify specific differential phosphorylation of K_v2.1 (bottom, lilac), from the dataset in (C). Data is mean \pm S.E.M., * $p < 0.05$, analysed by 2-tailed paired t-test. N = 5 animals, cultures from a single animal used to generate each paired sham and US exposed sample.

Figure 4. Ultrasound-induced modulation of K_v channel function requires ionotropic glutamate receptor activation. (A) Ingenuity Pathway Analysis showing the 5 most significantly modulated pathways ($p < 0.05$) in ultrasound exposed neuronal proteomes. Grayscale heatmap indicates t test–derived $-\log_{10}$ statistical P value. Coloured heatmap indicates the average expression level of each detected protein represented in individual boxes. Red indicates upregulation, blue indicates downregulation. (B-D) Quantification of synapse density and size. Representative confocal images from sham (top) and ultrasound (bottom) exposed neurons. Cultures are multiplex immunostained for MAP2, Synapsin and PSD-95. Scale bars = 10 μ m. There were no significant differences in (C) synapse density or (D) puncta size between sham and ultrasound exposed neurons. (E-G) Ultrasound exposure induces functional increases in excitatory synaptic transmission. (E) Representative 10 sec

trace segments displaying miniature excitatory postsynaptic currents (mEPSCs) recorded from sham (blue, top) and ultrasound (orange, bottom) exposed neurons. (F,G) Cumulative probability plots of (F) mEPSC frequency, as measured by inter-event interval, and (G) mEPSC amplitude, N = 1624 and 5368 events for control and ultrasound respectively. Insets display box plots of mean frequency and amplitude of mEPSCs for individual neurons. Line represents median, boxes are inter-quartile range, bars are min to max, analysed by Mann-Whitney U test. N = 23 and 21 neurons for control and ultrasound respectively. (H-I) Blocking glutamatergic synaptic activity blocks ultrasound induced modulation of whole cell potassium currents. (H) Representative current responses to 500ms voltage steps recorded from sham + vehicle (veh) (grey), sham + AP5 / NBQX (pink), US + veh (blue), and US + AP5 / NBQX (green), exposed cells. (I) I-V response curves derived from peak current magnitude, demonstrating glutamate receptor blockade inhibits ultrasound induced increases in current magnitude. Analysed by 2-tailed unpaired t-test with Holm-Sidak correction for multiple comparisons. N = 10 neurons per condition. *p < 0.05, **p < 0.01, ****p < 0.0001

Supplementary Figure 1. Axis-symmetric finite element model of the piezoelectric transducer and the petri dish system. (a) Geometry of the finite element model and the boundary conditions used to simulate the experiment. The right-hand boundaries were modelled as radiation boundaries to remove reflections and simulate the larger volume of the petri dish. (b) The resulting acoustic pressure of the acoustic field in model (a) which was 0.39MPa at the upper surface of the glass cover slide. (c) Geometry of a further finite element model with the lower boundary set as radiating to simulate a much larger depth of water which will remove any standing waves. (d) The resulting pressure of the acoustic field in model (c) which was 0.12MPa at the upper surface of the glass cover slide.

Figure 1

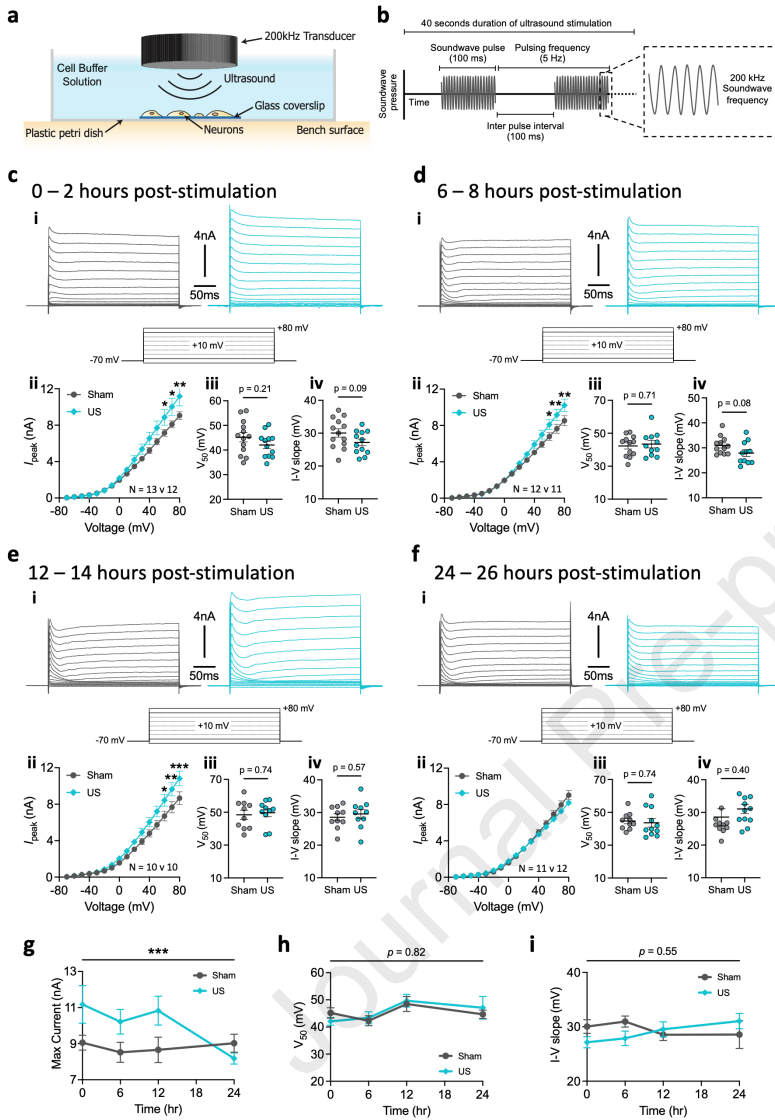


Figure 2

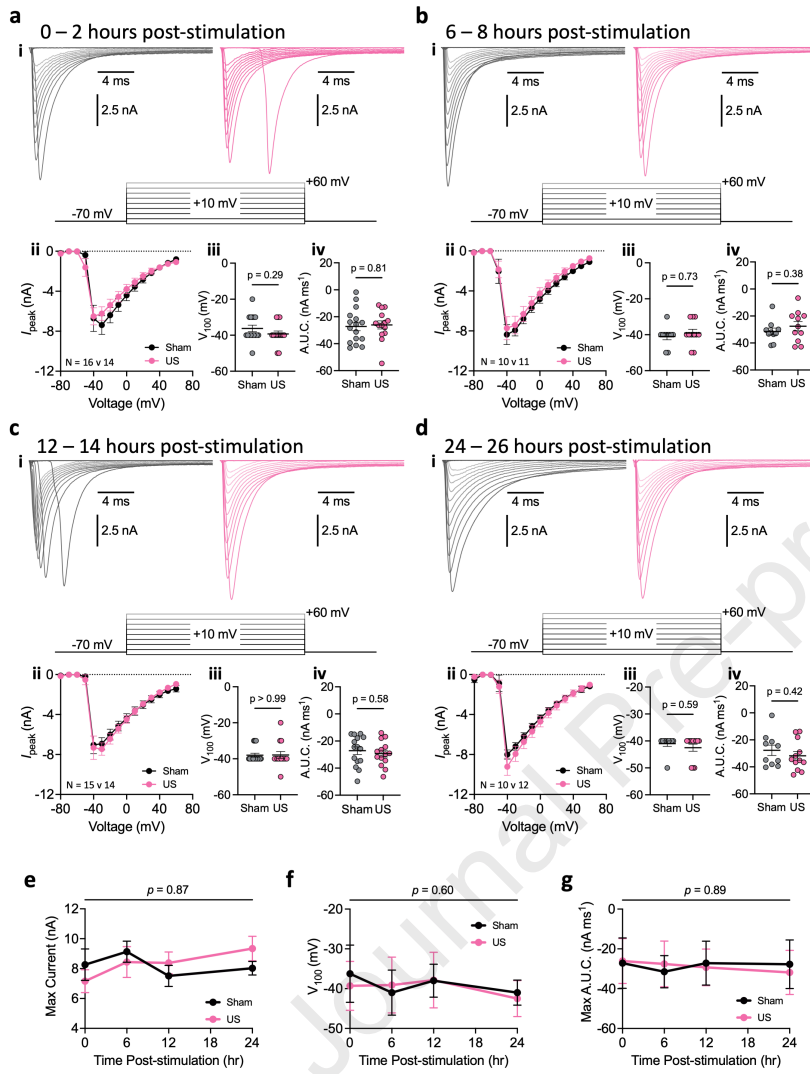


Figure 3

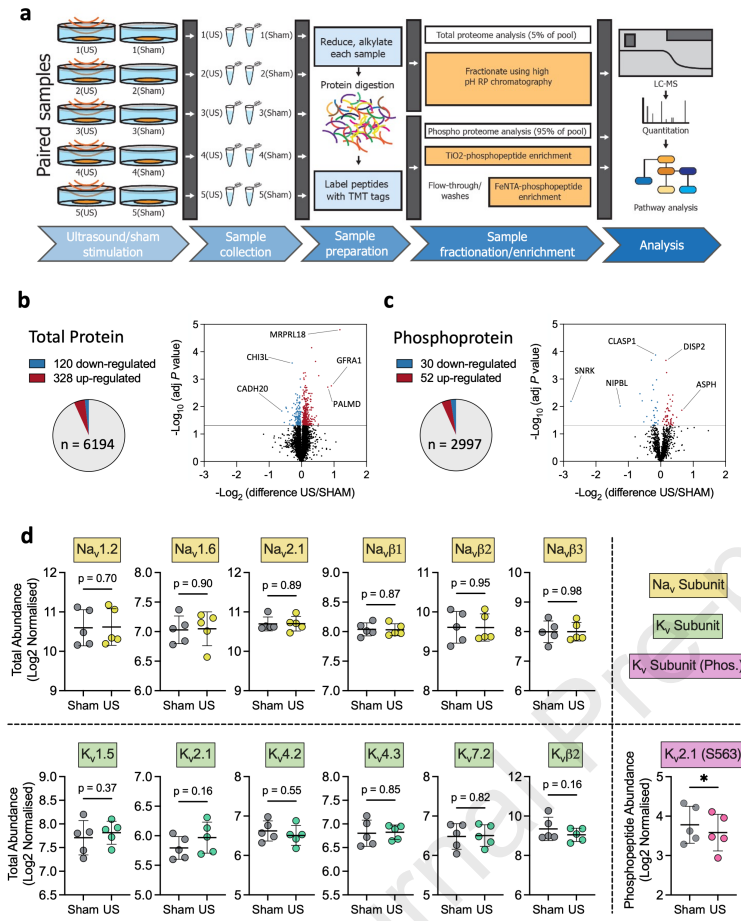
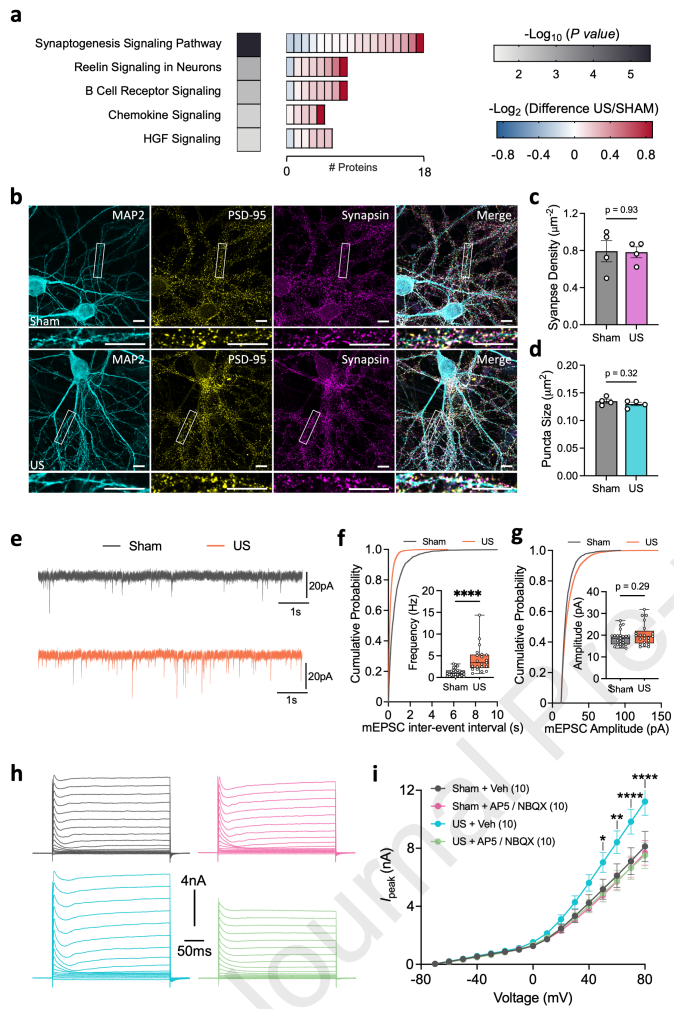


Figure 4



Highlights

- 40 s of ultrasound stimulation increases amplitude of voltage-gated K⁺ currents in cultured rat neurons.
- Voltage-gated K⁺ current modulation persists > 12 hours following stimulation.
- Quantitative proteomics implicates K_v2.1-specific dephosphorylation.
- Ultrasound stimulation induces synaptic signalling cascades and increases excitatory synaptic transmission.
- Inhibition of ionotropic glutamate receptor activation prevents ultrasound-induced modulation of voltage-gated K⁺ currents.

Journal Pre-proof

Declaration of interests

The authors declare that they have no known competing financial interests or personal relationships that could have appeared to influence the work reported in this paper.

The authors declare the following financial interests/personal relationships which may be considered as potential competing interests:

Journal Pre-proof